Supplement of The Cryosphere, 17, 4571–4599, 2023
https://doi.org/10.5194/tc-17-4571-2023-supplement

The Cryosphere Open Access EGU

Supplement of

The evolution of future Antarctic surface melt using PISM-dEBM-simple

Julius Garbe et al.

Correspondence to: Julius Garbe (julius.garbe@pik-potsdam.de)

List of supplementary tables

List of supplementary figures

Table S1. List of ice-sheet model constants and parameters used in PISM and their default values adopted for this study.

Symbol	Parameter	Value	Unit
Δx, Δy	Horizontal grid resolution	8	km
Δz	Vertical grid resolution	$13-87$	m
n	Glen flow law exponent	3	–
E_{SIA}	Enhancement factor for SIA	1	–
E_{SSA}	Enhancement factor for SSA	1	–
u_0	Sliding law threshold velocity (Eq. (1))	100	$\mathrm{m\,yr^{-1}}$
q	Pseudo-plastic sliding exponent (Eq. (1))	0.75	–
c_0	Apparent till cohesion (Eq. (2))	0	Pa
$\phi_{\min}$	Minimal till friction angle (Eq. (3))	2	°
$\phi_{\max}$	Maximal till friction angle (Eq. (3))	50	°
$b_{\min}$	Bed elevation of $\phi_{\min}$ (Eq. (3))	-700	m
$b_{\max}$	Bed elevation of $\phi_{\max}$ (Eq. (3))	500	m
$W_{\max}$	Maximal water thickness in till (Eq. (4))	2	m
C_d	Till water drainage rate (Eq. (4))	7	$\mathrm{mm\,yr^{-1}}$
N_0	Reference effective till pressure (Eq. (5))	1,000	Pa
e_0	Reference void ratio at N_0 (Eq. (5))	0.69	–
C_c	Till compressibility (Eq. (5))	0.12	–
δ	Lower bound of N, as fraction of overburden pressure (Eq. (5))	0.04	–
T_{s}	Temperature of snow precipitation	273.15	K
T_{r}	Temperature of rain precipitation	275.15	K
f_{s}	Degree-day factor for snow	3.3	$\mathrm{mm\,w.e.\,(PDD)^{-1}}$
f_{i}	Degree-day factor for ice	8.8	$\mathrm{mm\,w.e.\,(PDD)^{-1}}$
Γ	Atmospheric temperature lapse rate	-8.2	$\mathrm{K\,km^{-1}}$
C	PICO overturning strength	1	$\mathrm{Sv\,m^3\,kg^{-1}}$
γ_T	PICO vertical heat exchange coefficient	$3\cdot10^{-5}$	$\mathrm{m\,s^{-1}}$
K	Eigencalving coefficient	$1\cdot10^{16}$	m s
H_{cr}	Thickness threshold for calving	50	m

PDD, positive degree-day.

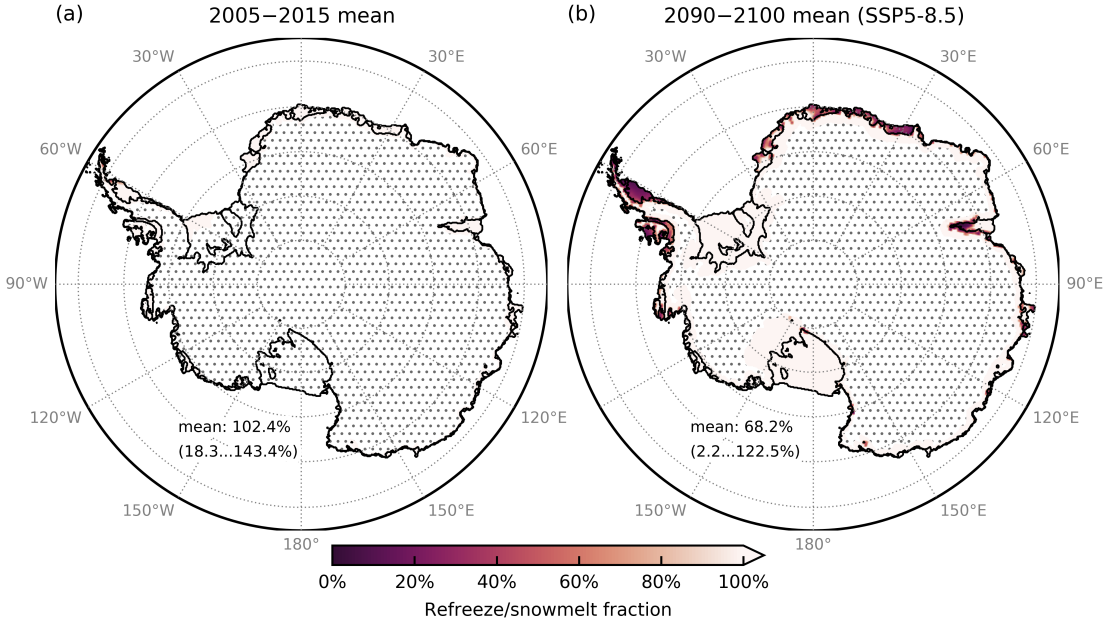

Figure S1. Refreeze-per-melt fraction in RACMO. Ratio of decadal mean refreezing and snow melt fluxes in RACMO2.3p2 (in percent) as an approximation for the refreeze fraction parameter θ used in PISM-dEBM-simple, shown for present day (2005–2015 mean) (**a**) and the end of the century (2090–2100 mean), assuming an SSP5-8.5 warming scenario (**b**). Values given in each panel denote the mean and respective range (minimum–maximum), calculated over the ice shelves and masking all areas where annual mean surface melt is small (< 10 mm w.e. yr^{-1}; hatched) in order to avoid numerical artifacts.

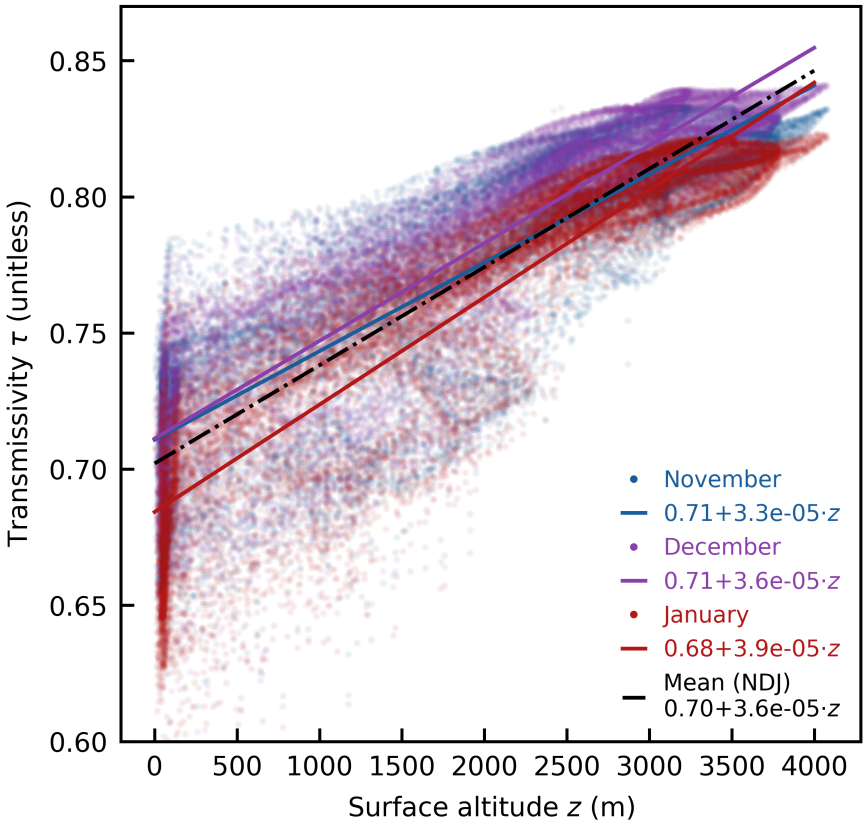

Figure S2. Linear regression fit for the parameterization of atmospheric transmissivity. Atmospheric transmissivity τ (unitless) over the Antarctic Ice Sheet versus ice-sheet surface altitude z (in m), given by multi-year monthly means of RACMO2.3p2 data over the historical period (1950–2015) computed on RACMO's native 27 km grid. The transmissivity is calculated from the ratio of incident shortwave solar radiation at the ice surface and the top of the atmosphere (TOA). A linear regression fit is shown for each of the three austral summer months with the highest average TOA insolation (November, December and January; NDJ) (colored solid lines) with best-fit parameters given in the legend. The transmissivity parameterization in dEBM-simple (Eq. (7)) uses best-fit parameters (intercept $a_\tau = 0.70$ and slope $b_\tau = 3.6 \cdot 10^{-5}$ m^{-1}) of the linear fit resulting from the mean over those three months (black dash-dotted line). Best-fit parameters from the November, December and January regression fits serve as uncertainty estimates in the model sensitivity ensemble (Sect. 5.4).

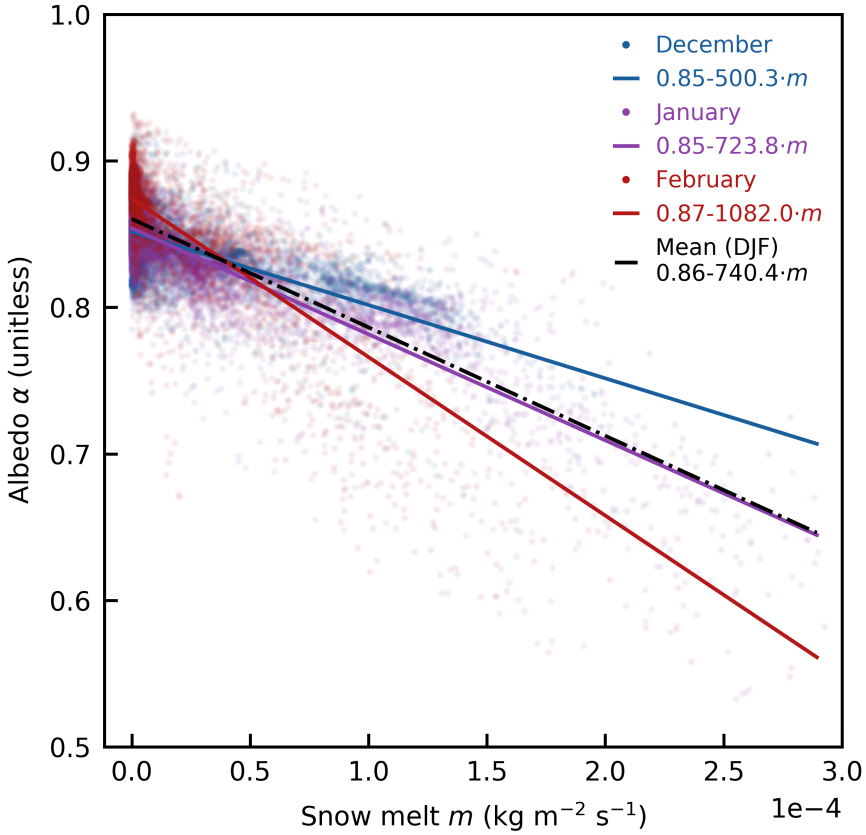

Figure S3. Linear regression fit for the parameterization of surface albedo. Antarctic surface albedo α (unitless) versus snow melt m (in $\mathrm{kg\,m^{-2}\,s^{-1}}$), given by multi-year monthly means of RACMO2.3p2 data over the period 2085 to 2100 under the SSP5-8.5 warming scenario provided by CESM2, computed on RACMO's native 27 km grid. A linear regression fit is shown for each of the three austral summer months with the highest average melt (December, January, February; DJF) (colored solid lines) with best-fit parameters given in the legend. The albedo parameterization in dEBM-simple (Eq. (8)) uses best-fit parameters (intercept $a_\alpha = 0.86$ and slope $b_\alpha = -740.4\ [\mathrm{kg\,m^{-2}\,s^{-1}}]^{-1}$) of the linear fit resulting from the mean over those three months (black dash-dotted line). Best-fit parameters from the December, January and February regression fits serve as uncertainty estimates in the model sensitivity ensemble (Sect. 5.4). Grid cells where the mean albedo is below the allowed minimum value $\alpha_{\min} = 0.47$ and grid cells which show melt even below the allowed minimum temperature $T_{\min} = -10\ ^\circ\mathrm{C}$ have been masked before the fits.

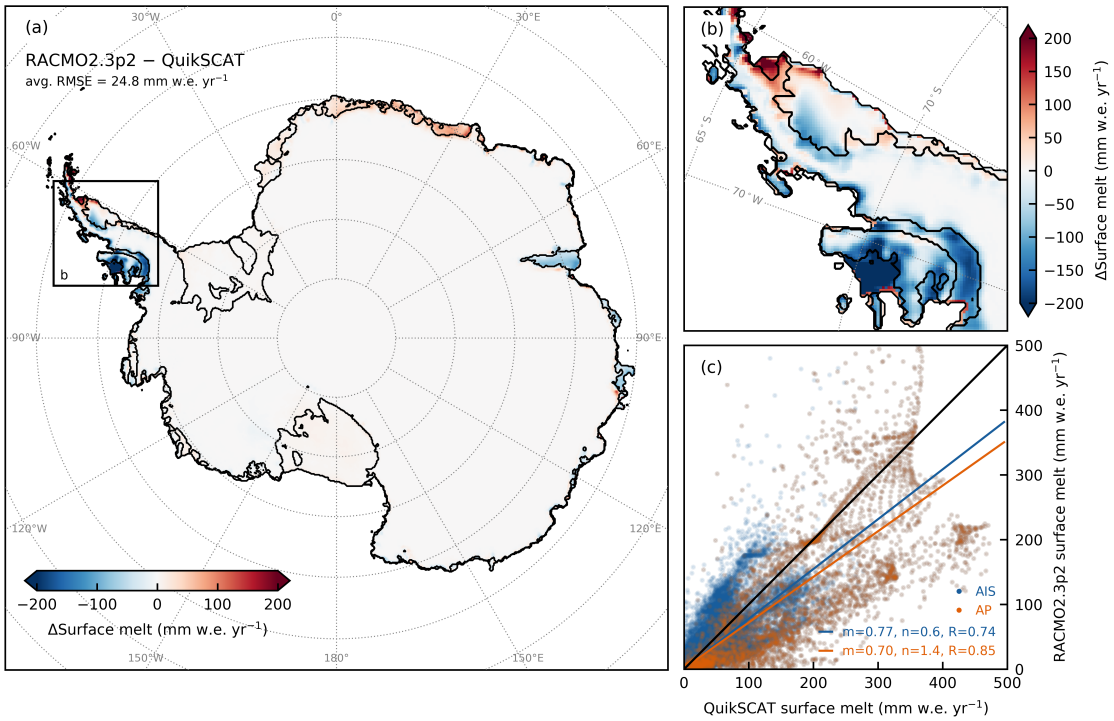

Figure S4. Comparison of present-day (2000–2009) mean Antarctic surface melt rates from RACMO with satellite-based meltwater flux estimates. (**a**) Map of Antarctic surface melt rate difference (in millimeters water equivalent per year, mm w.e. yr^{-1}) between RACMO2.3p2-CESM2 and satellite-based meltwater flux estimates derived from QuikSCAT data (Trusel et al., 2013), average over the period 2000 to 2009. The root-mean-square error (RMSE), averaged across the entire ice sheet, is also given. (**b**) Same as panel (a), shown for a zoomed-in section of the Antarctic Peninsula, the region with the highest average melt rates, indicated by the black square in panel (a). (**c**) Scatter plot of RACMO versus QuikSCAT-based surface melt estimates (in mm w.e. yr^{-1}) and linear regression fits of the data (colored solid lines). Blue data points correspond to the whole Antarctic Ice Sheet (AIS), orange data points to the zoomed-in section of the Antarctic Peninsula (AP) shown in panel (b). m and n are the slope and intercept of the regression lines, respectively, and R is the Pearson correlation coefficient. The black line marks the identity line.

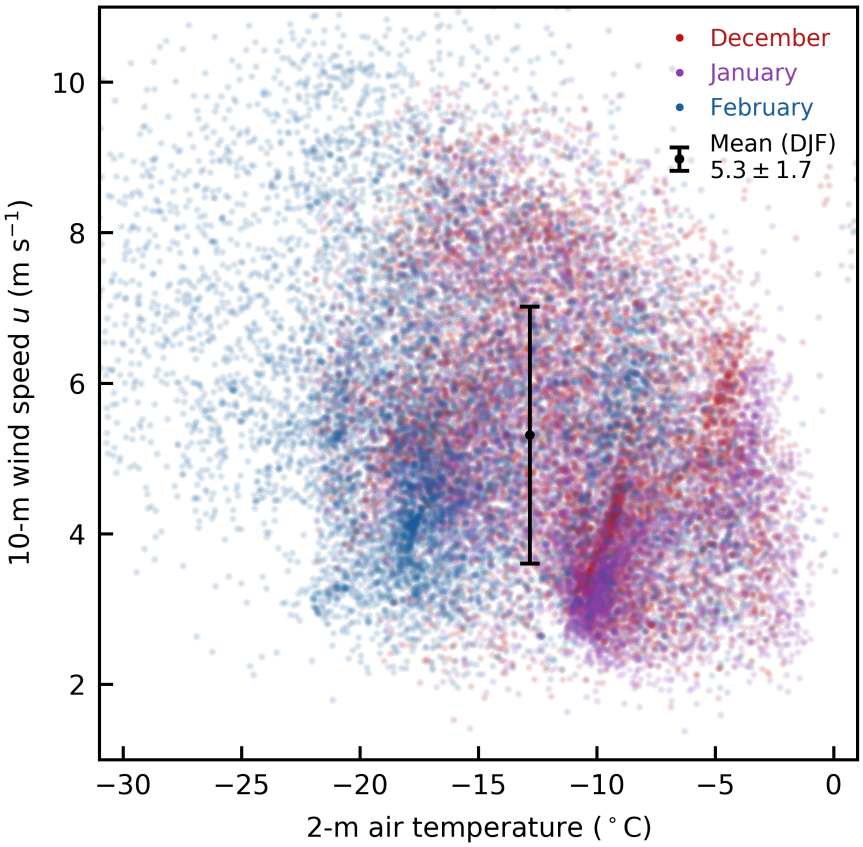

Figure S5. Average summer wind speeds over the lower parts of the Antarctic Ice Sheet. Wind speed at 10 m above ground u (in $\mathrm{m\,s^{-1}}$) during the austral summer months December, January and February (DJF) over the lower parts of the Antarctic Ice Sheet (elevations < 2000 m) versus near-surface (2 m) air temperature (in °C), given by multi-year monthly means of RACMO2.3p2 data over the historical period (1950–2015), computed on RACMO's native 27 km grid. The black dot marks the DJF mean (value given in the legend) that is used in the estimation of the dEBM-simple tuning parameter c_1 for the best-guess value. The error bars denote the standard deviation.

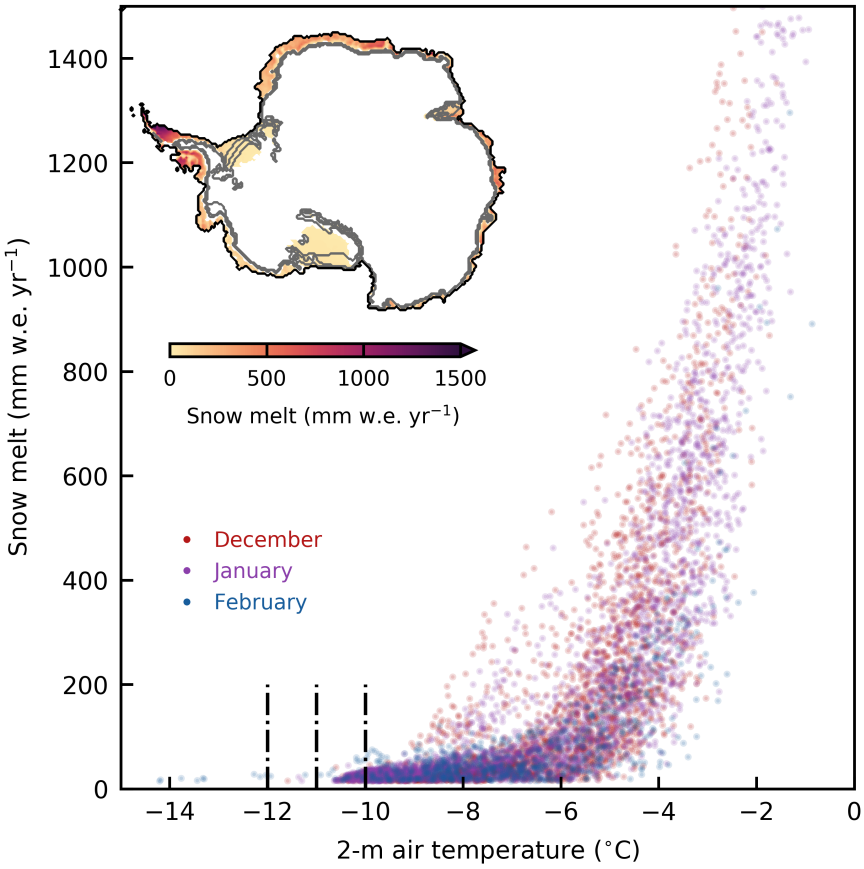

Figure S6. Threshold temperature for melt. Antarctic snow melt rates (in mm w.e. yr^{-1}) as a function of near-surface air temperature (in °C), given by multi-year monthly means of RACMO2.3p2 data over the historical period (1950–2015) for the austral summer months with the highest average melt (December–February; DJF), computed on RACMO's native 27 km grid. The black dash-dotted lines mark the temperature values that are used in the calibration as estimates of the threshold temperature T_{min}, which constitutes the background melt condition in dEBM-simple. They mark the approximate long-term monthly mean temperature range above which significant surface melt occurs in the RACMO simulations. The inset shows a map of the spatial distribution of 1950 to 2015 multi-year mean DJF Antarctic snow melt rates from RACMO. The gray contour lines mark the -10, -11, -12 °C isotherms of long-term mean summer air temperatures (1950–2015 DJF mean), respectively, that roughly approximate the mean extent of the melt area.

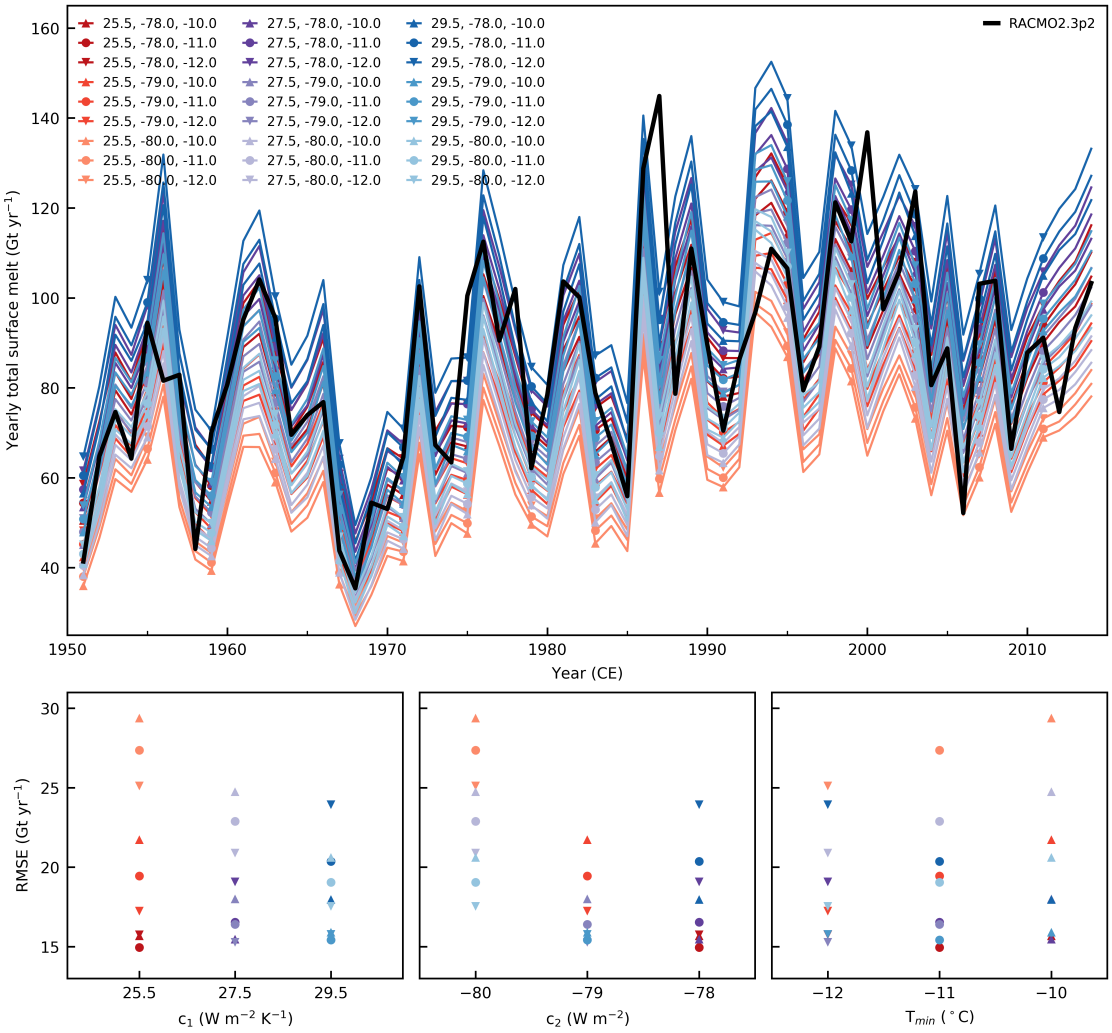

Figure S7. Yearly total Antarctic surface melt in the historical model calibration ensemble. Upper panel shows the evolution of Antarctic-wide integrated yearly total surface melt flux (in gigatons per year, Gt yr^{-1}) as calculated with PISM-dEBM-simple in the historical (1950–2015) model calibration ensemble using a fixed geometry (colored lines). The number tuples in the legend are $\{c_1$ (in W m^{-2} K^{-1}), c_2 (in W m^{-2}), $T_{\min}$ (in °C)$\}$. The black line shows the yearly total surface melt flux derived with RACMO2.3p2 under boundary forcing from CESM2, bilinearly regridded to PISM's 8 km grid using a common surface mask. Lower panels show the respective temporal root-mean-square error (RMSE, in Gt yr^{-1}) of each model ensemble member with respect to RACMO, individually plotted against c_1 (left), c_2 (middle), and $T_{\min}$ (right).

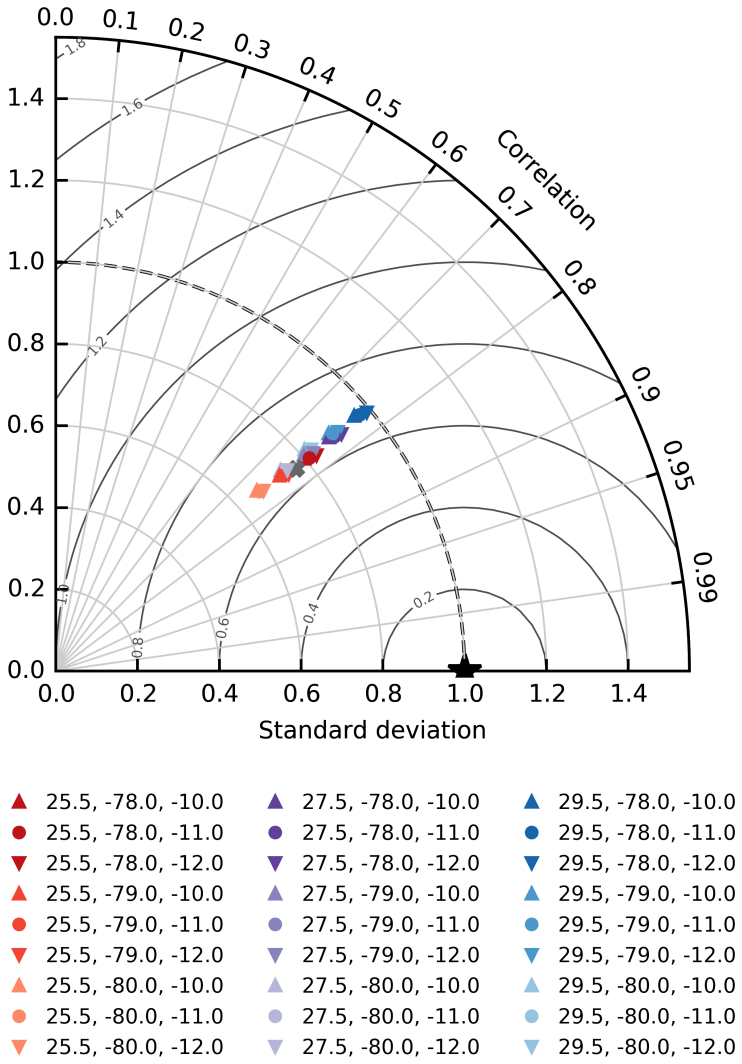

Figure S8. Taylor diagram summarizing the performance of the historical model calibration ensemble. The diagram shows a summary of the performance of each ensemble member from the historical model calibration ensemble (colored markers; legend entries as in Fig. S7) compared to the Antarctic-wide integrated yearly total surface melt flux from RACMO2.3p2 (black pentagram). The horizontal and vertical axes represent the standard deviation, normalized with respect to the standard deviation of the RACMO surface melt flux (bold dashed black line). The azimuthal angle shows the correlation between the individual ensemble members and RACMO, given by the Pearson correlation coefficient. Finally, the (normalized) centered root-mean-square error, representing a bias-corrected equivalent of the root-mean-square error, is given by the circular dark gray contour lines. The gray cross marker shows the performance of PISM using the standard PDD scheme for comparison.

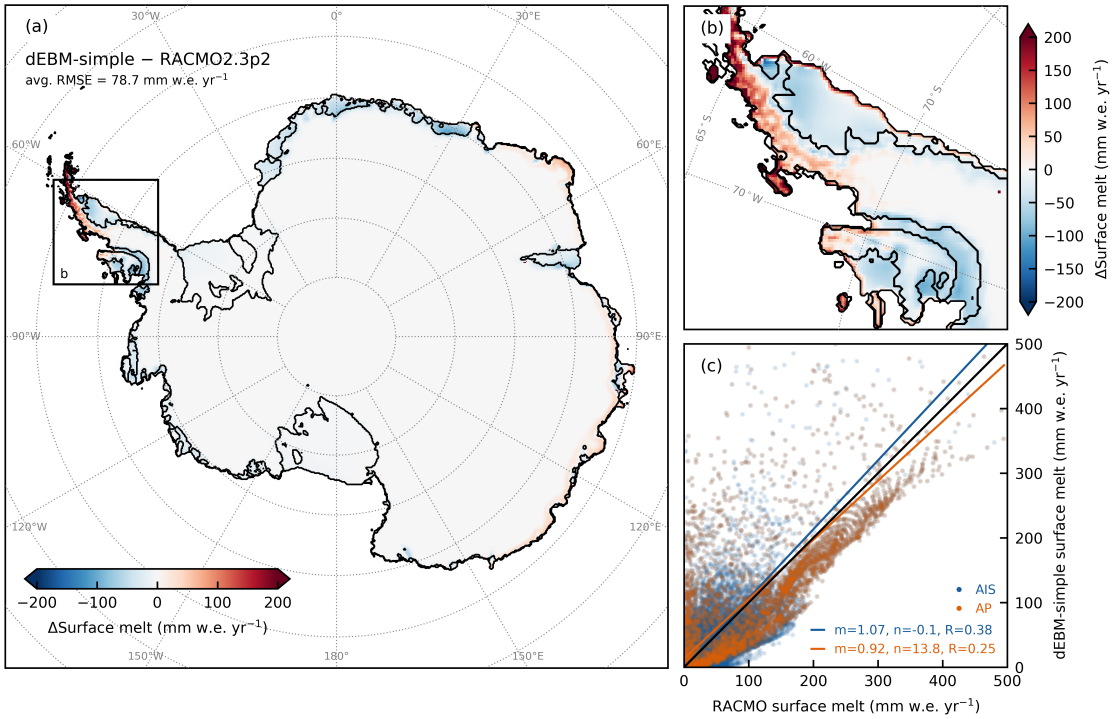

Figure S9. Comparison of historical (1950–2015 mean) Antarctic surface melt rates between dEBM-simple and RACMO. (**a**) Map of absolute difference of dEBM-simple minus RACMO-computed surface melt rates (in mm w.e. yr^{-1}), averaged over the historical period (1950–2015). The root-mean-square error (RMSE), averaged across the entire ice sheet, is also given. (**b**) Zoomed-in section of the Antarctic Peninsula, the region with the highest average melt rates, indicated by the black square in panel (a). (**c**) Scatter plot of dEBM-simple versus RACMO-computed surface melt rates (in mm w.e. yr^{-1}) and linear regression fits of the data (colored solid lines). Blue data points correspond to the whole Antarctic Ice Sheet (AIS), orange data points to the zoomed-in section of the Antarctic Peninsula (AP) shown in panel (b). m and n are the slope and intercept of the regression lines, respectively, and R is the Pearson correlation coefficient. The black line marks the identity line.

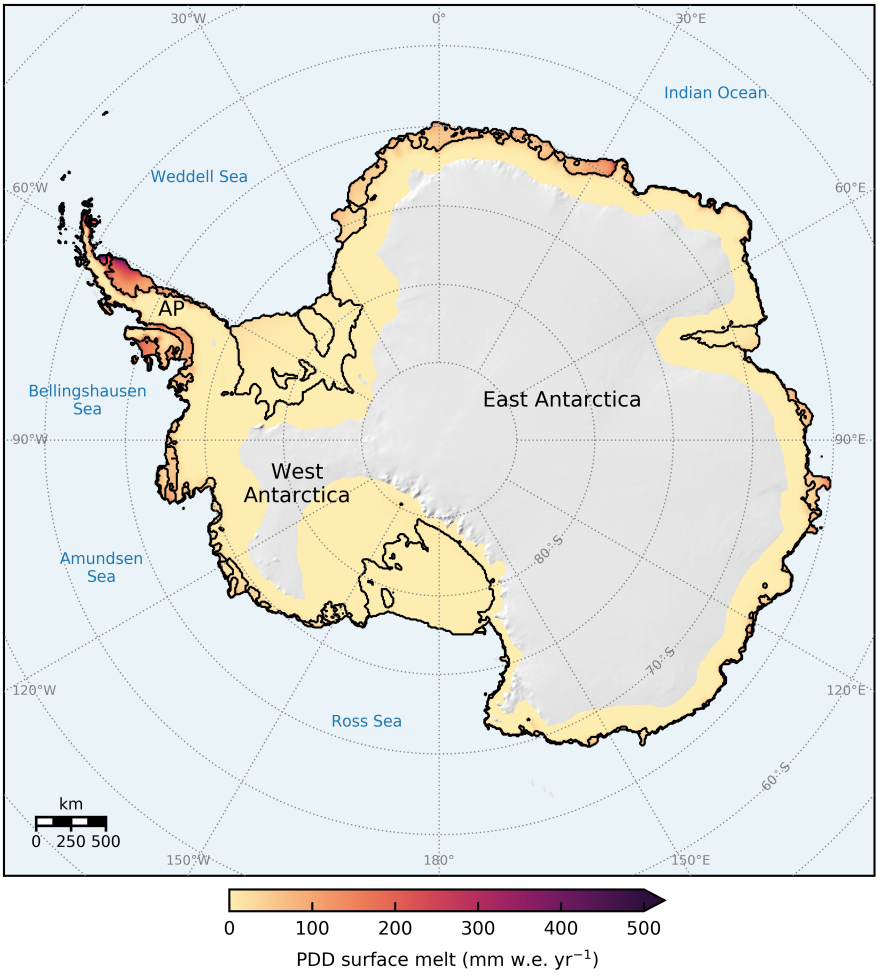

Figure S10. Present-day (2005–2015 mean) Antarctic surface melt rates computed with PISM using PDD. Map of Antarctic surface melt rates (in mm w.e. yr^{-1}), as calculated with PISM using a standard PDD scheme, averaged over the period 2005 to 2015. Areas with melt rates below numerical significance (< 0.001 mm w.e. yr^{-1}) are masked. AP, Antarctic Peninsula.

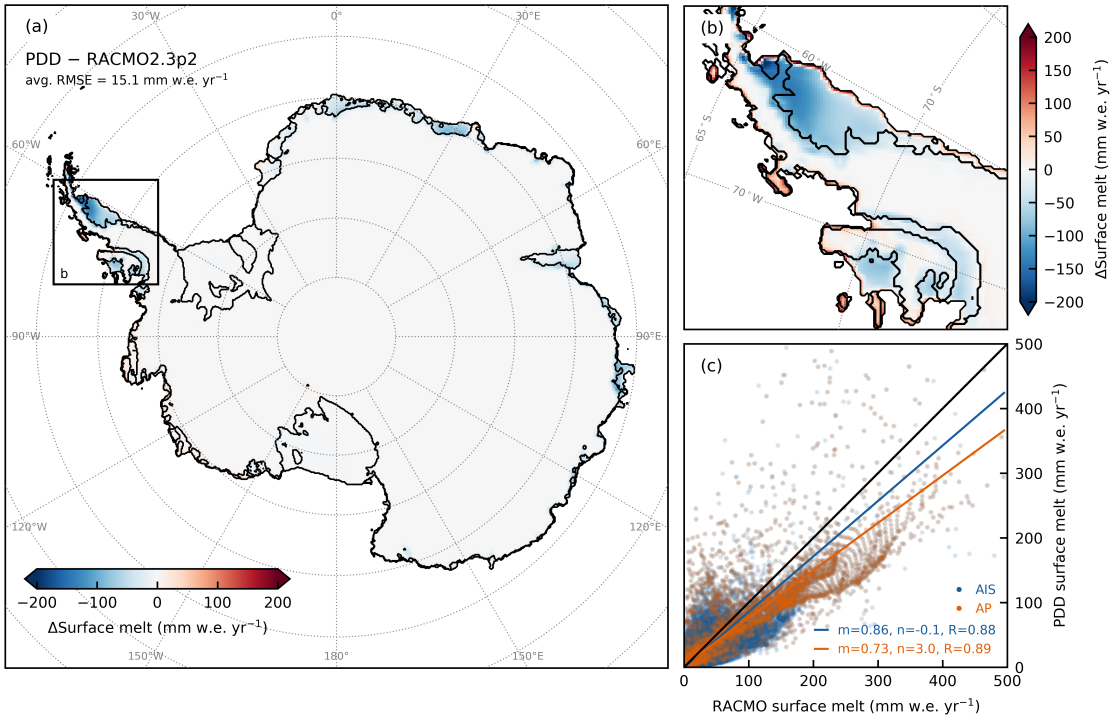

Figure S11. Comparison of historical (1950–2015 mean) Antarctic surface melt rates between PDD and RACMO. Same as Fig. S9, but for PISM using a standard PDD melt scheme. (**a**) Map of absolute difference of PDD minus RACMO-computed surface melt rates (in mm w.e. yr^{-1}), averaged over the historical period (1950–2015). The root-mean-square error (RMSE), averaged across the entire ice sheet, is also given. (**b**) Zoomed-in section of the Antarctic Peninsula, the region with the highest average melt rates, indicated by the black square in panel (a). (**c**) Scatter plot of PDD versus RACMO-computed surface melt rates (in mm w.e. yr^{-1}) and linear regression fits of the data (colored solid lines). Blue data points correspond to the whole Antarctic Ice Sheet (AIS), orange data points to the zoomed-in section of the Antarctic Peninsula (AP) shown in panel (b). m and n are the slope and intercept of the regression lines, respectively, and R is the Pearson correlation coefficient. The black line marks the identity line.

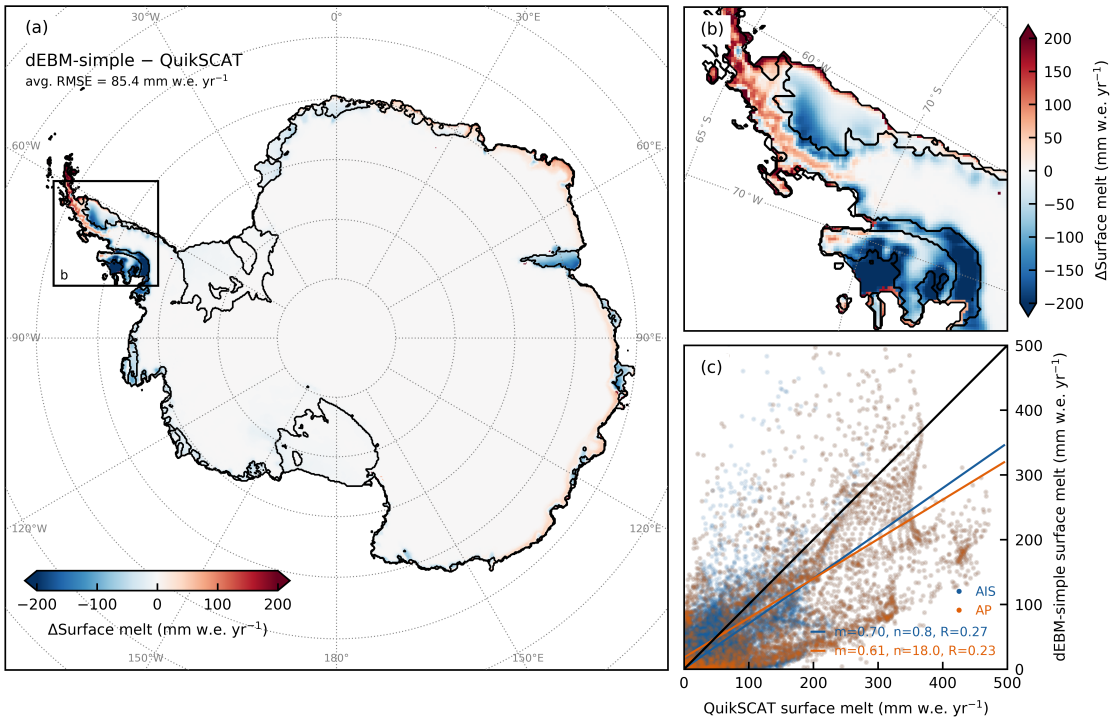

Figure S12. Comparison of present-day (2000–2009 mean) Antarctic surface melt rates from dEBM-simple with satellite-based meltwater flux estimates. (**a**) Map of Antarctic surface melt rate difference (in mm w.e. yr^{-1}) between PISM-dEBM-simple and satellite-based meltwater flux estimates derived from QuikSCAT data (Trusel et al., 2013), average over the period 2000 to 2009. The root-mean-square error (RMSE), averaged across the entire ice sheet, is also given. (**b**) Same as panel (a), shown for a zoomed-in section of the Antarctic Peninsula, the region with the highest average melt rates, indicated by the black square in panel (a). (**c**) Scatter plot of dEBM-simple versus QuikSCAT-based surface melt estimates (in mm w.e. yr^{-1}) and linear regression fits of the data (colored solid lines). Blue data points correspond to the whole Antarctic Ice Sheet (AIS), orange data points to the zoomed-in section of the Antarctic Peninsula (AP) shown in panel (b). m and n are the slope and intercept of the regression lines, respectively, and R is the Pearson correlation coefficient. The black line marks the identity line.

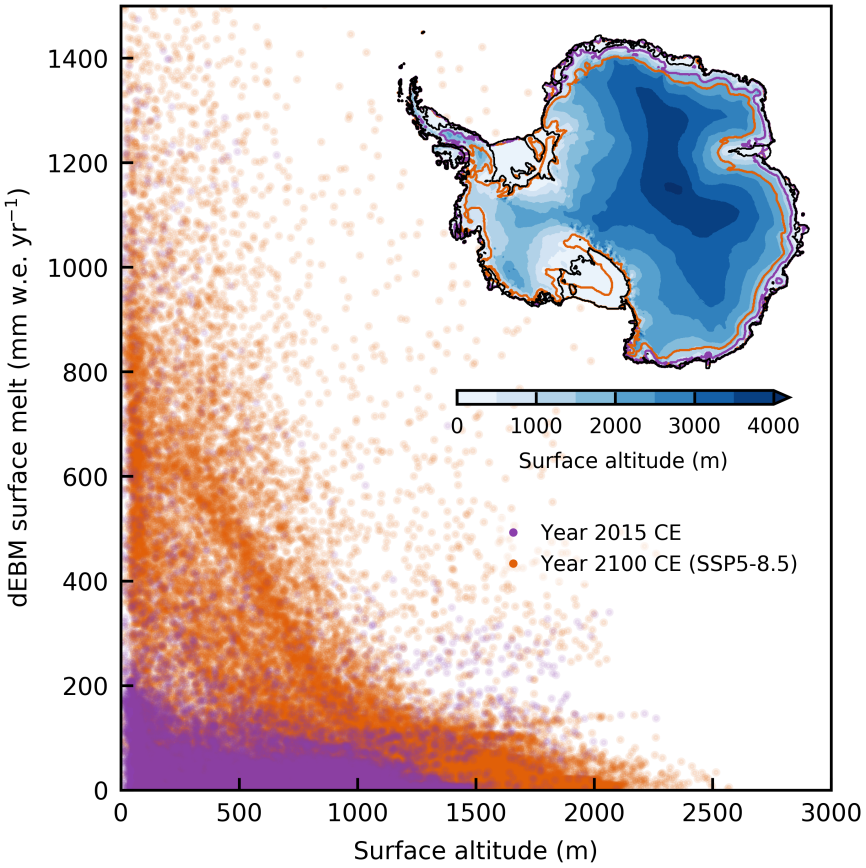

Figure S13. Surface melt rates as a function of the ice-sheet surface altitude. Antarctic surface melt rates (in mm w.e. yr^{-1}) over the grounded parts of the ice sheet as computed with PISM-dEBM-simple, shown as a function of ice-sheet surface altitude for present day (year 2015; purple data points) and the year 2100, assuming an SSP5-8.5 atmospheric warming scenario (orange data points). The inset map shows the maximum extent of the melt area at the two respective times as colored contours, overlaid on the present-day ice-sheet surface altitude (contour levels of 500 m).

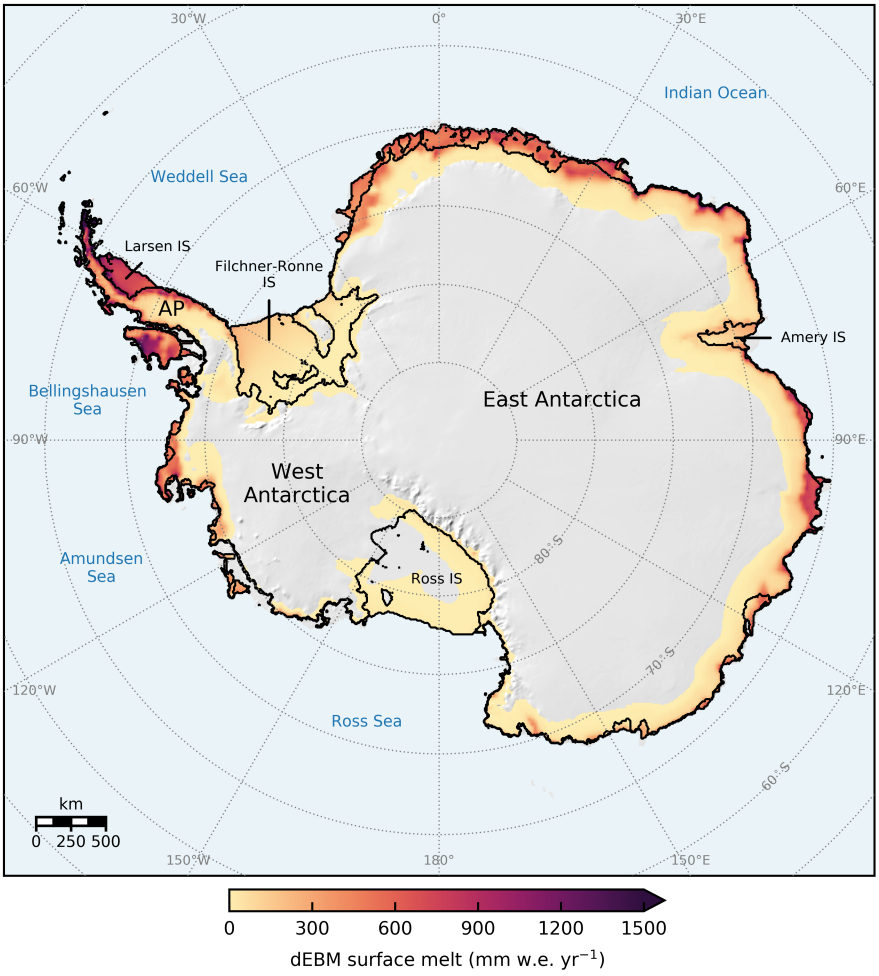

Figure S14. End-of-century (2090–2100 mean) Antarctic surface melt rates computed by dEBM-simple. Map of Antarctic surface melt rates (in mm w.e. yr^{-1}), as calculated with PISM-dEBM-simple in the calibrated 21st-century projection run forced by RACMO2.3p2 with atmospheric boundary forcing from CESM2 and following an SSP5-8.5 warming scenario, averaged over the period 2090 to 2100. Areas with melt rates below numerical significance (< 0.001 mm w.e. yr^{-1}) are masked. AP, Antarctic Peninsula. Note that the axis limits are different from those in Fig. 2a.

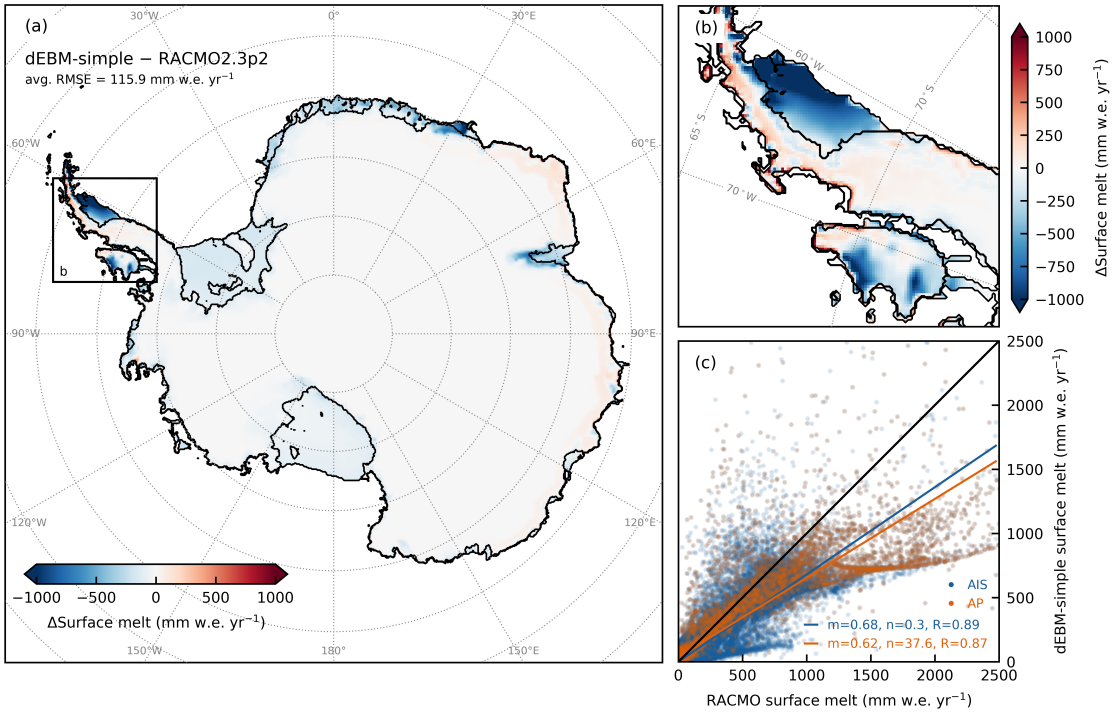

Figure S15. Comparison of end-of-century (2090–2100 mean) Antarctic surface melt rates between dEBM-simple and RACMO. (**a**) Map of absolute difference of dEBM-simple minus RACMO-computed surface melt rates (in mm w.e. yr^{-1}) as calculated with PISM-dEBM-simple in the calibrated 21st-century projection run forced by RACMO2.3p2 with atmospheric boundary forcing from CESM2 and following an SSP5-8.5 warming scenario, averaged over the period 2090 to 2100. The root-mean-square error (RMSE), averaged across the entire ice sheet, is also given. (**b**) Zoomed-in section of the Antarctic Peninsula, the region with the highest average melt rates, indicated by the black square in panel (a). (**c**) Scatter plot of dEBM-simple versus RACMO-computed surface melt rates (in mm w.e. yr^{-1}) and linear regression fits of the data (colored solid lines). Blue data points correspond to the whole Antarctic Ice Sheet (AIS), orange data points to the zoomed-in section of the Antarctic Peninsula (AP) shown in panel (b). m and n are the slope and intercept of the regression lines, respectively, and R is the Pearson correlation coefficient. The black line marks the identity line. Note that the axis limits in all panels are different from those in Fig. S9.

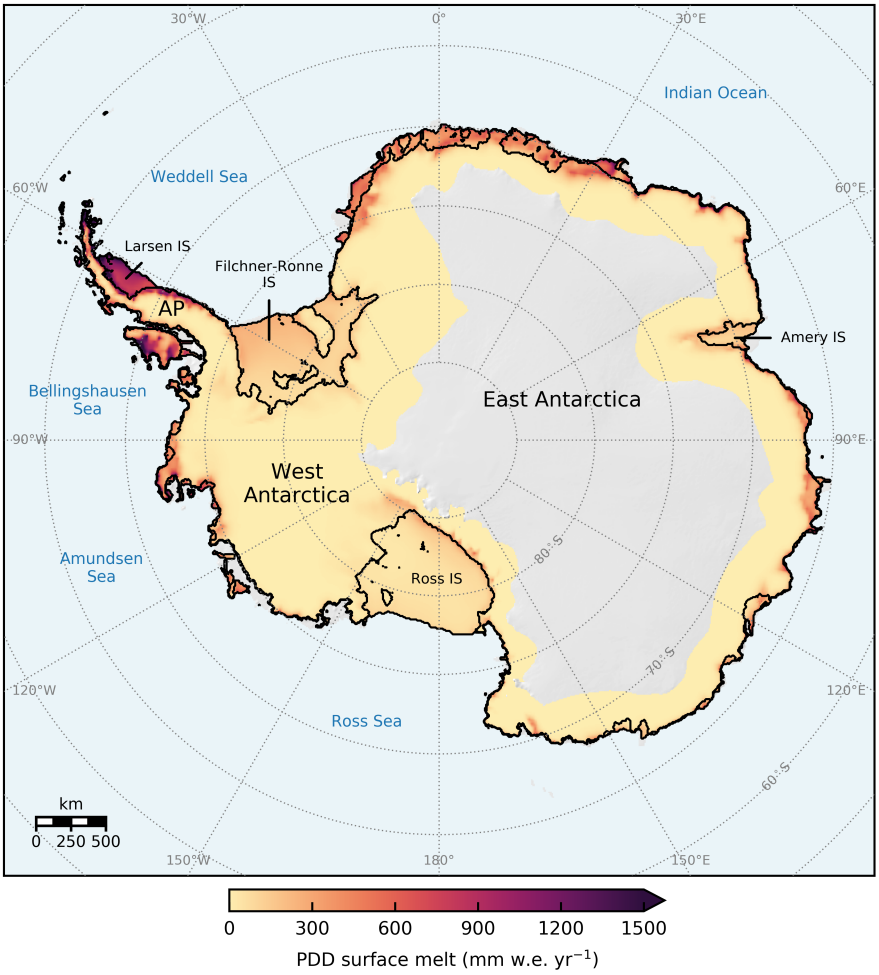

Figure S16. End-of-century (2090–2100 mean) Antarctic surface melt rates computed with PISM using PDD. Same as Fig. S14, but computed with PISM using a standard PDD melt scheme.

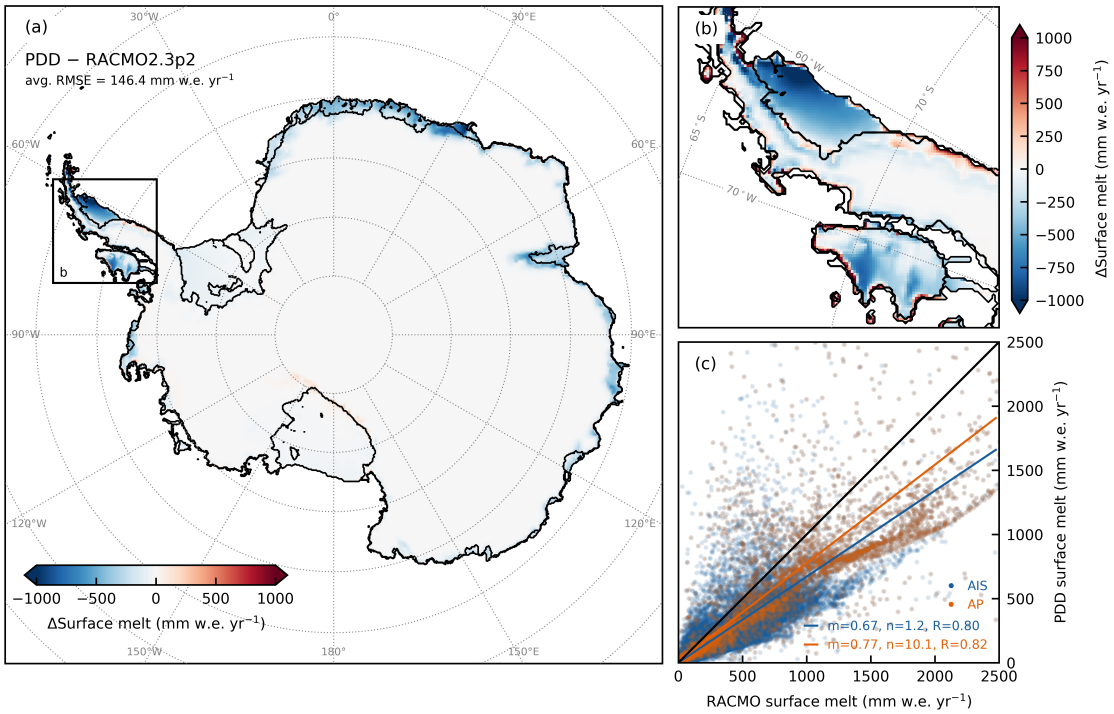

Figure S17. Comparison of end-of-century (2090–2100 mean) Antarctic surface melt rates between PDD and RACMO. Same as Fig. S16, but computed with PISM using a standard PDD melt scheme.

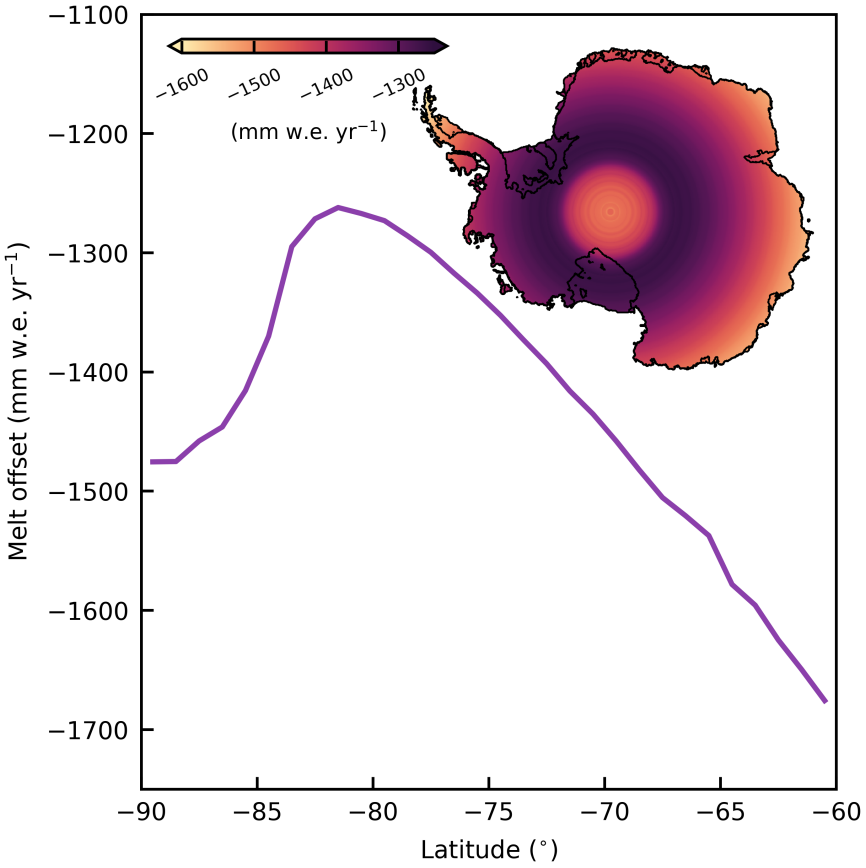

Figure S18. Melt offset M_{off}. Annual average (negative) surface melt potential $M_{\text{off}} \propto c_2$ (in mm w.e. yr^{-1}) resulting from outgoing longwave radiation (third term in Eq. (6)), which acts as a negative offset to the total surface melt flux, as a function of latitude. Inset map shows the spatial distribution.

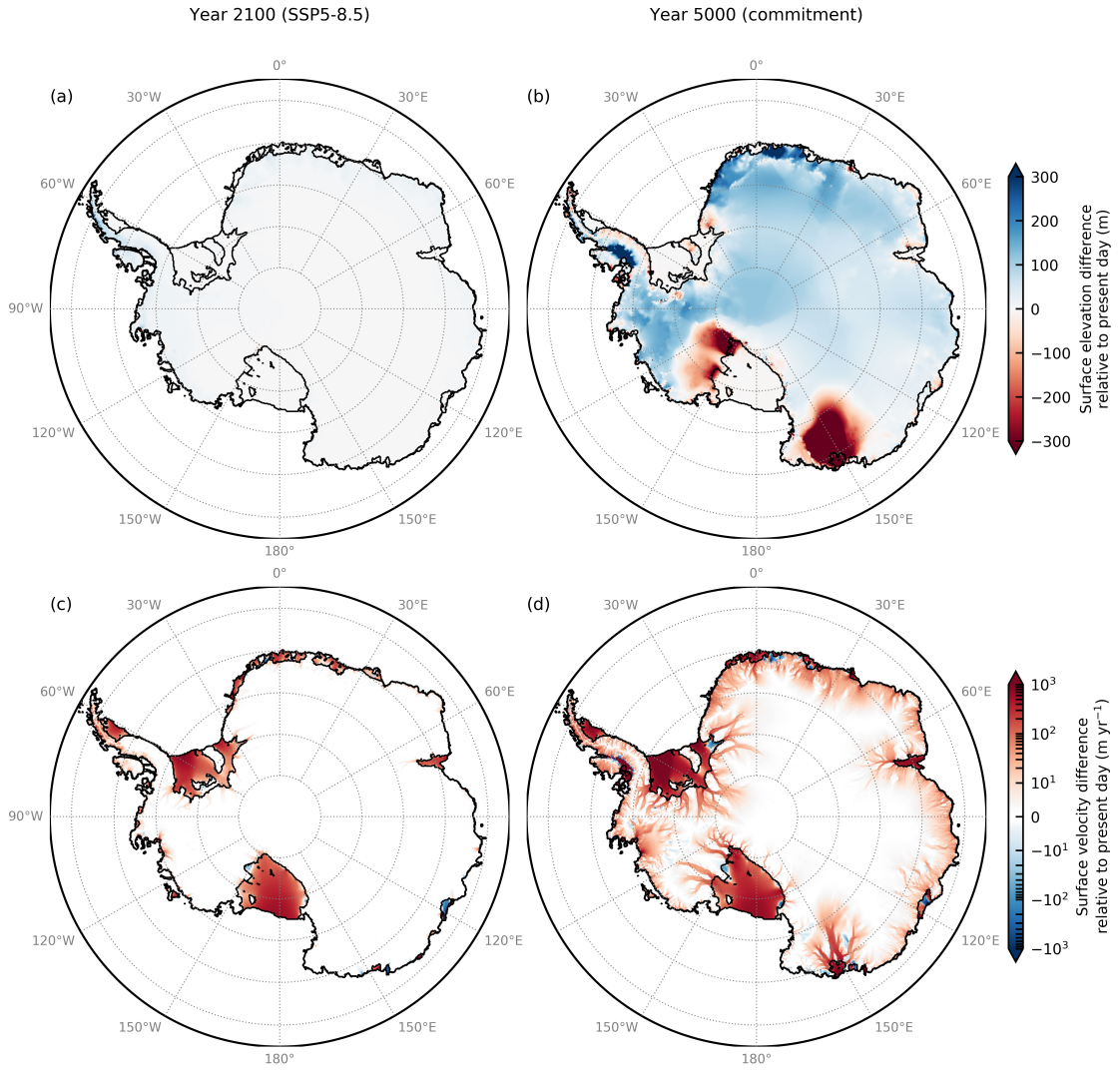

Figure S19. Committed dynamical changes in Antarctica resulting from enhanced surface melting. Same as Fig. 6, but assuming a constant refreeze fraction of $\theta = 0.9$. Shown is the difference in ice-sheet surface elevation (in m) as modeled with PISM-dEBM-simple under SSP5-8.5 forcing from RACMO2.3p2 compared to a control simulation run under present day (1986–2015 mean) conditions (**a**) in 2100 and (**b**) under sustained end-of-century (2090–2100 monthly mean) climate conditions in the year 5000. (**c–d**) Same as panels (a–b), but for ice surface velocity (in m yr^{-1}).

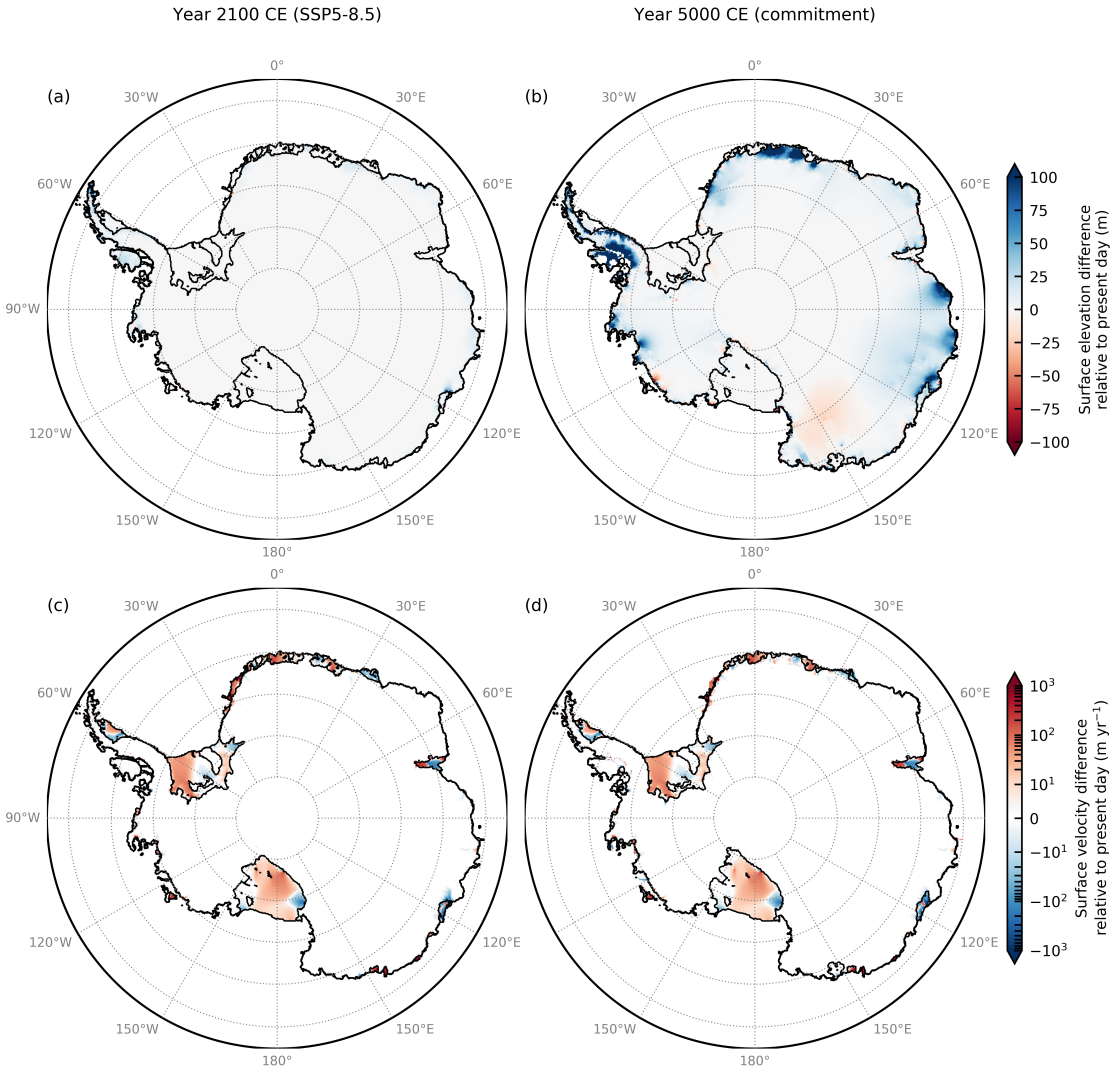

Figure S20. Uncertainty of committed dynamical changes in Antarctica resulting from enhanced surface melting. Difference between committed ice-dynamical changes with respect to present day assuming a constant refreeze fraction of $\theta = 0.9$ (i.e., Fig. S19) minus committed ice-dynamical changes assuming a constant refreeze fraction of $\theta = 0.5$ (i.e., Fig. 6). Variables and units as in Fig. 6, but note the different range of the color scale in panels (a) and (b).

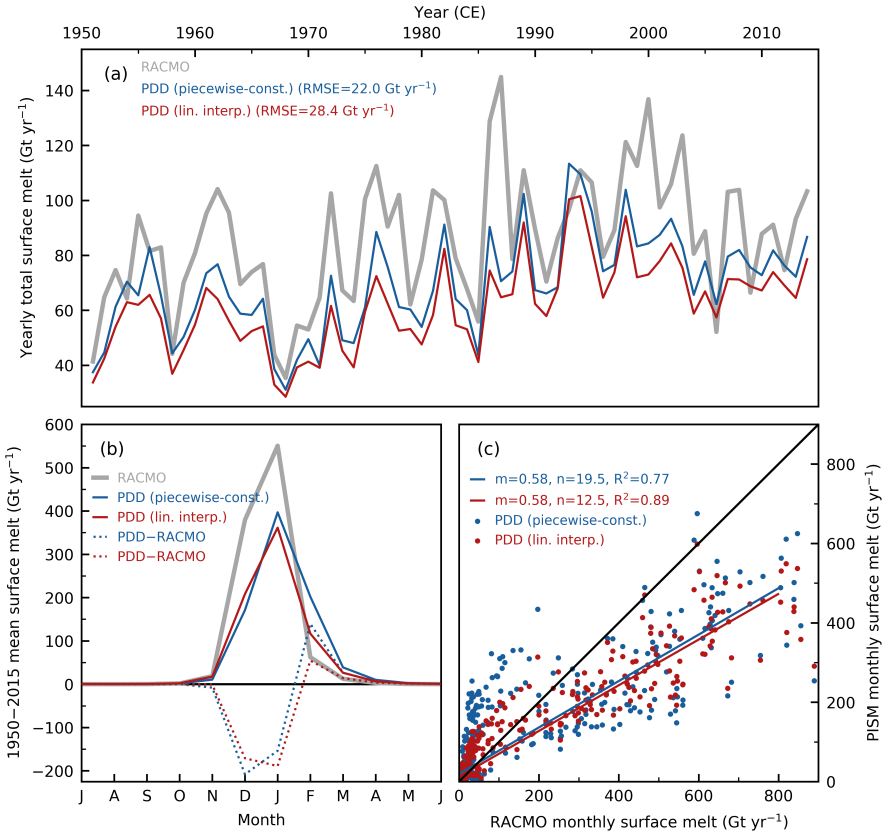

Figure S21. Impacts of temperature forcing treatment on PDD-derived melt. Same as Fig. 1, but comparing RACMO-derived melt fluxes with PDD-derived melt fluxes with and without applying a linear interpolation between the monthly air temperature forcing inputs in PISM. (**a**) Antarctic-wide integrated 1950 to 2015 yearly total surface melt flux (in gigatons per year, Gt yr^{-1}) as calculated with a standard PDD melt scheme using piecewise-constant temperature forcings (blue line; default) and linearly interpolating between the monthly temperature inputs (red line). The light gray line shows the yearly melt flux predicted by RACMO2.3p2. The root-mean-square errors (RMSE) of yearly total melt fluxes with respect to RACMO are given in parentheses. (**b**) Multi-year monthly averaged annual melt cycle (in Gt yr^{-1}) for PDD with piecewise-constant (blue) and linearly interpolated (red) monthly temperature inputs compared to RACMO (solid light gray line). The dotted lines show the respective differences between PDD and RACMO. (**c**) Total monthly surface melt fluxes from PDD with piecewise-constant (blue) and linearly interpolated (red) temperature inputs in comparison to RACMO melt fluxes (in Gt yr^{-1}) and linear regression fit of the data (colored solid lines). m and n are the slope and intercept of the regression lines, respectively, and R^2 the coefficient of determination. The black line marks the identity line.

References

Trusel, L. D., Frey, K. E., Das, S. B., Munneke, P. K., and Broeke, M. R.: Satellite-based estimates of Antarctic surface meltwater fluxes, Geophysical Research Letters, 40, 6148–6153, 2013.